

Multi-Touch and Bending Perception Using Electrical Impedance Tomography for Robotics

Haofeng Chen¹, Bedrich Himmel¹, Bin Li², Xiaojie Wang², Matej Hoffmann¹

Abstract—Electrical Impedance Tomography (EIT) offers a promising solution for distributed tactile sensing with minimal wiring and full-surface coverage in robotic applications. However, EIT-based tactile sensors face significant challenges during surface bending. Deformation alters the baseline impedance distribution and couples with touch-induced conductivity variations, complicating signal interpretation. To address this challenge, we present a novel sensing framework that integrates a deep neural network for interaction state classification with a dynamic adaptive reference strategy to decouple touch and deformation signals, while a data-driven regression model translates EIT voltage changes into continuous bending angles. The framework is validated using a magnetic hydrogel composite sensor that conforms to bendable surfaces. Experimental evaluations demonstrate that the proposed framework achieves precise and robust bending angle estimation, high accuracy in distinguishing touch, bending, and idle states, and significantly improves touch localization quality under bending deformation compared to conventional fixed-reference methods. Real-time experiments confirm the system’s capability to reliably detect multi-touch interactions and track bending angles across varying deformation conditions. This work paves the way for flexible EIT-based robotic skins capable of rich multimodal sensing in robotics and human–robot interaction.

I. INTRODUCTION

The importance of endowing robots with touch has been recognized for several decades and a large number of technologies have been developed (e.g., [1], [2] for surveys). The focus has largely been on tactile sensing for manipulation, as equipping robot fingers or hands with tactile sensors requires only relatively small patches of electronic skin. Whole-body artificial skins for robots have been an exception, with only few successful solutions such as [3], [4]. The potential of sensing over the whole body surface has also not been fully explored. Cheng et al. provide an overview of applications of their electronic skin in [5].

Even for the so-called whole-body skins [5], [6], it is not the complete surface of the robot that is covered. In particular the areas around the robot joints are typically without skin coverage. Complete coverage would be desired for both physical and social human-robot interaction [7], [8]. The main challenge for articulated robots lies in sustaining large deformation and stretch while still delivering

¹Haofeng Chen, Bedrich Himmel, Matej Hoffmann are with the Department of Cybernetics, Faculty of Electrical Engineering, Czech Technical University in Prague.

²Bin Li and Xiaojie Wang are with the Institute of Intelligent Machines, Hefei Institutes of Physical Science, Chinese Academy of Sciences, Hefei 230031, China.

This work was co-funded by the European Union under the project Robotics and Advanced Industrial Production (reg. no. CZ.02.01.01/00/22.008/0004590).

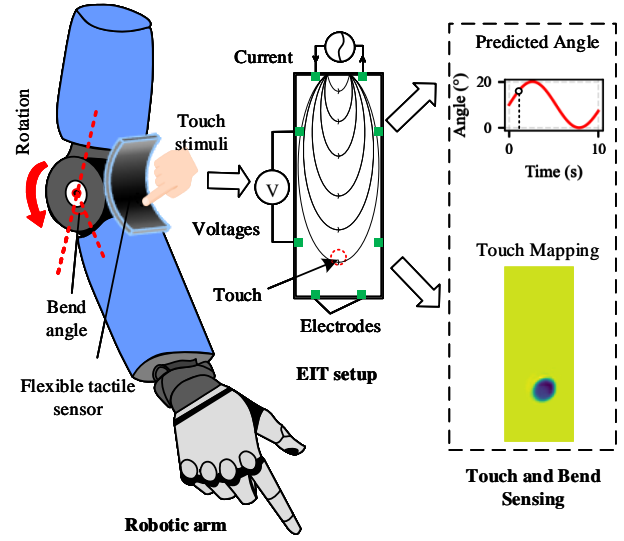


Fig. 1: Overview of EIT-based flexible tactile sensor for touch and bending sensing.

touch information. While measuring the angle of deformation (bending) may not be key for classical robots, which have accurate joint encoders, bending information may be relevant in soft robots, providing valuable information about their body configuration (see e.g., [9]).

While flexible tactile sensors have been explored, few achieve both high-resolution touch and bending measurement. For example, Noda et al. [10] introduced a stretchable liquid-based tactile sensor with a dual-channel design to detect bending and touch, but its low spatial resolution limits multi-touch sensing. Totaro et al. [11] proposed a multimodal mechanosensing system using resistive and optical components, capable of distinguishing between pressure and bending, but limited to single-point touch and complex in design due to multi-principle integration. Sarwar et al. [12] developed a capacitive sensor array capable of detecting multi-touch during bending and stretching, but it does not explicitly decouple touch and deformation signals and lacks quantitative bending estimation. Zhang et al. [13] designed a microwave-based sensor capable of sensing both pressure and bending, but its small sensing area and electromagnetic coupling mechanism limit scalability for large-area applications. Overall, most sensors capable of touch and bending measurement compromise between spatial resolution, multi-touch capability, and signal decoupling, making it difficult to achieve both high-resolution touch and bending measure-

ment. As the sensing area increases, the growing number of sensors adds wiring and interface complexity, along with higher costs.

EIT presents a promising alternative for distributed sensing without requiring multiple discrete sensor units, making it well suited for whole-body robotic applications. Prior research has explored EIT for touch sensing, such as Kato et al. [20], who developed a soft, pressure-sensitive EIT-based tactile sensor for finger touch sensing. Nagakubo et al. [21] presented an early demonstration of EIT-based tactile sensing by attaching a conductive knit sensor to a dummy’s elbow. They applied pressure to one point under fully bent and fully extended postures, showing that EIT can detect touch on a deformable surface. However, their work focused on basic touch detection and did not explore continuous bending sensing or the interaction between touch and bending. Yu et al. [17] developed uKnit, a scarf-like soft wearable sensor combining machine knitting with EIT. The system demonstrated worn-location detection, gesture recognition, and respiratory monitoring, highlighting EIT’s potential for flexible and reconfigurable sensing. However, its design faced challenges such as limited spatial resolution and signal anisotropy due to the knitted fabric structure, which constrains sensing precision. Park et al. [19] introduced a large-area, face-shaped EIT sensor for multi-touch recognition.

EIT has also been applied to shape sensing in soft robots, with Avery et al. [22] and Xin et al. [16] using it to map deformations in real time. However, these approaches lack touch sensing, limiting their practicality for real-time applications. Dong et al. [18] demonstrated 3D-scanner-assisted EIT for tactile interaction mapping on deformable surfaces, but their approach required complex hardware and was not suitable for real-time applications. Despite these advancements, few studies have addressed the sensing of touch and bend in large-deformation robotic applications using EIT. Table I summarizes recent developments in flexible tactile sensors capable of touch and/or bend sensing.

The primary challenge in achieving both touch and bending sensing using EIT lies in signal coupling—both touch and bending alter the impedance distribution in a complex manner, making it difficult to separate their effects. Additionally, EIT is an ill-posed inverse problem, where small measurement variations can lead to significant reconstruction errors, especially under substantial deformations.

To address these limitations, this paper presents an EIT-based sensing framework capable of both real-time multi-touch detection and bending angle estimation, with enhanced touch resolution even after significant deformation of the sensor surface. Figure 1 is an illustration of the flexible tactile sensor on a robot joint, enabling it to track bending angles and localize touch positions through conductivity distribution analysis. EIT reconstructs internal conductivity patterns by applying electrical currents and measuring boundary voltages via surface electrodes. Touch interactions generate localized conductivity mapping, whereas bending leads to distributed measurement variations due to geometric deformation. The

deformation information can be leveraged to enhance touch localization and enable accurate bending estimation.

The key contributions of this work are summarized as follows: (1) We propose a novel sensing framework based on EIT that enables both localization of multi-touch events and estimation of bending angles on a single flexible sensor surface.

(2) To address the signal coupling between touch and bending, we introduce a dynamic adaptive reference strategy that updates reconstruction references based on the deformation state, enhancing touch localization resolution under large surface deformations.

(3) We design and implement a large-area, conformable EIT sensor suitable for robotic integration, capable of maintaining high spatial resolution across different bending configurations.

(4) We demonstrate real-time performance of the proposed system in experiments involving sequential bending and touch inputs, validating its robustness and effectiveness for interactive robotic applications.

II. METHODS AND SYSTEM DESIGN

The proposed method enables sensing of touch and bend based on EIT signals. As shown in Figure 2, the framework comprises three main stages: state classification, reference signal management, and extraction of touch and bend information. Our system is built around time-difference EIT modeling, which estimates conductivity changes $\Delta\sigma$ from changes in boundary voltage $\Delta\mathbf{V}$ across temporal states. This model serves as a foundational transformation across all processing stages, including feature extraction, classification, and touch mapping.

A. Time-Difference EIT Modeling

The EIT problem involves reconstructing the internal conductivity distribution of a conductive domain based on applied currents and measured boundary voltages. We use a time-difference formulation [23] to emphasize temporal changes in conductivity between a reference and observed state. In difference imaging, the connection between the change in conductivity, $\Delta\sigma \in \mathbb{R}^N$, and the change in measured voltage, $\Delta\mathbf{V} \in \mathbb{R}^M$, can be approximated as a linear relationship:

$$\Delta\mathbf{V} = \mathbf{J}\Delta\sigma + \mathbf{n}_{noise} \quad (1)$$

where $\mathbf{J} \in \mathbb{R}^{M \times N}$ ($M \ll N$) is the sensitivity (Jacobian) matrix, calculated via the finite element method (FEM), $\mathbf{n}_{noise} \in \mathbb{R}^M$ accounts for measurement noise. We define the conductivity change vector as $\Delta\sigma = [\Delta\sigma_1, \Delta\sigma_2, \dots, \Delta\sigma_N]$, where $\Delta\sigma_i = \sigma_i - \sigma_0$. Here, σ_0 is the background conductivity, and σ_i is the conductivity of the i -th element. Similarly, the voltage change vector $\Delta\mathbf{V} = [\Delta v_1, \Delta v_2, \dots, \Delta v_M]$ is calculated as $\Delta v_i = v_i - v_i^{ref}$, where $\mathbf{V}^{ref} = [v_1^{ref}, v_2^{ref}, \dots, v_M^{ref}]$ is the reference voltage vector and $\mathbf{V} = [v_1, v_2, \dots, v_M]$ is the current voltage

TABLE I: Comparison of recent flexible tactile sensors supporting touch or bending sensing.

Study	Sensing Method	Touch & Bend	Multi-Touch	High touch resolution	Area	Flexible
Sarwar et al. [12]	Capacitive	Yes	Yes	No	55 × 55 mm	Yes
Kim et al. [14]	Optical + Piezoresistive	Yes	No	No	70 × 10 mm	Yes
Lee et al. [15]	Resistance	No (Bend only)	No	No	10 × 10 mm	Yes
Xin et al. [16]	EIT	No (Bend only)	No	No	60 × 20 mm	Yes
Zhang et al. [13]	Microwave	Yes	No	No	95 × 58 mm	Yes
Yu et al. [17]	EIT	Yes	No	No	~952 cm ²	Yes
Dong et al. [18]	EIT + 3D Scan	No (Touch only)	Yes	Yes	150 × 100 mm	Yes
Park et al. [19]	EIT	No (Touch only)	Yes	Yes	314 mm ²	No
This Work	EIT	Yes	Yes	Yes	150 × 60 mm	Yes

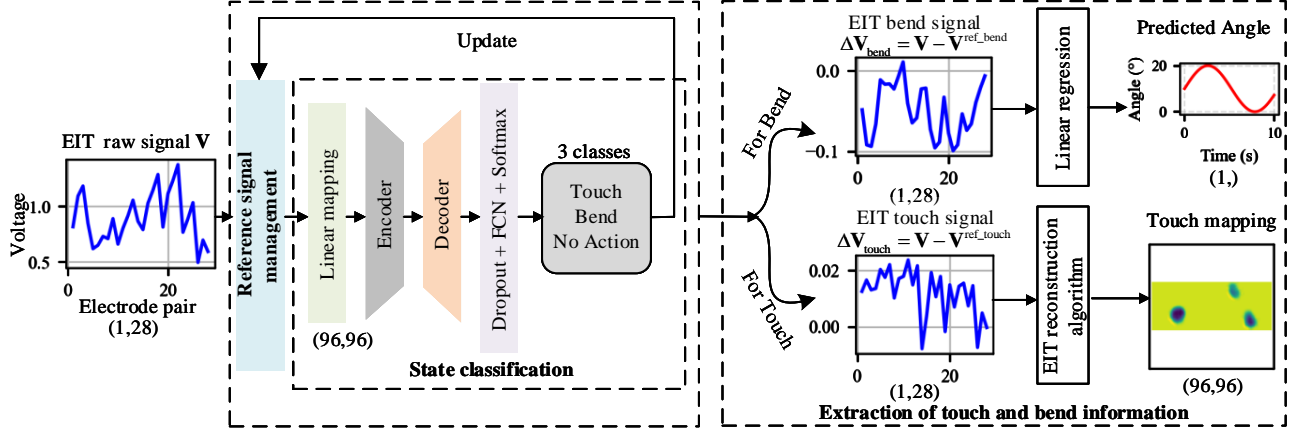


Fig. 2: Overview of the proposed framework for multi-touch and bending sensing.

vector. To solve the inverse problem, we employ the one-step Gauss-Newton method [24]:

$$\Delta\sigma = (\mathbf{J}^T \mathbf{J} + \lambda^2 \mathbf{R})^{-1} \mathbf{J}^T \Delta \mathbf{V} \quad (2)$$

where \mathbf{J}^T represents the transpose of the sensitivity matrix \mathbf{J} , λ is a scalar hyperparameter that controls the regularization strength, chosen heuristically. \mathbf{R} denotes the regularization matrix. The matrix \mathbf{R} is computed using Newton's One-Step Error Reconstructor (NOSER) prior [25]. This transformation is treated as a linear mapping in our neural pipeline and is also used for touch reconstruction after classification.

B. Reference signal management and state classification

In dynamic tactile applications, the sensor undergoes significant deformation, which affects the reference voltage readings. To ensure accurate differential imaging, we adopt a state-aware classification framework that also manages reference signal updates adaptively.

The pipeline begins with the sensor's raw voltage signal $\mathbf{V} \in \mathbb{R}^{1 \times 28}$, which is first processed by a reference signal management module (Figure 2). This module manages two types of reference voltages. The first is a static reference, denoted as $\mathbf{V}^{\text{ref},\text{bend}}$, acquired when the sensor is in its undeformed state and used as the reference for bending estimation. The second is a dynamic touch reference, denoted as $\mathbf{V}^{\text{ref},\text{touch}}$, which is recorded after deformation when a touch event is detected under bent conditions. For classification, the system compares the current voltage measurement with the static reference to obtain a differential signal that reflects internal conductivity changes.

This difference signal is then linearly projected into an image-like conductivity embedding $\Delta\sigma$ via Eq. (2). This transformation provides spatially meaningful features and reduces sensitivity to static boundary effects, allowing the classifier to focus on internal conductivity variations caused by touch or bending. The conductivity map is then fed into an encoder-decoder neural network for interaction classification. The encoder consists of three convolutional layers with kernel size 3×3 and progressively increasing feature dimensions from 16 to 32 and then to 64, interleaved with max-pooling and batch normalization layers. The decoder mirrors this structure using transposed convolutions and upsampling operations to restore spatial resolution. Finally, two fully connected layers reduce the representation to 16 dimensions, followed by a softmax layer that predicts the current sensor state as either touch, bend, or no action.

The classification result guides the reference management process. When a bending state is detected, the system retains the static reference for subsequent angle estimation. When a touch is detected under deformation, the dynamic reference is updated to enable accurate touch reconstruction. These references are then used in the following stage for bend angle prediction and touch mapping.

C. Bend angle prediction and Touch mapping

Task-specific EIT signals are extracted using bend reference for bending and touch reference for touch, forming the basis for subsequent modeling ((Figure 2)). To establish a quantitative relationship between sensor voltage changes and

bending angles, we adopted a data-driven approach combining feature selection and linear regression modeling from the scikit-learn library [26]. Given the high-dimensional nature of the EIT voltage response data, we performed feature selection using SelectKBest with *f_regression* scoring from Scikit-learn [26], leveraging the continuous nature of the bending angles. This process identified the most relevant voltage features based on their correlation with bending variations, effectively reducing dimensionality and focusing on the most informative signals. These selected features were then used to train a linear regression model, establishing a direct mapping between voltage changes and bending angles.

For touch mapping, the system employs the previously described one-step Gauss-Newton reconstruction algorithm to recover the conductivity distribution. To improve the spatial resolution and suppress reconstruction artifacts, a lightweight convolutional post-processing module is applied [27]. This module enhances the clarity of contact regions without significantly increasing computational cost.

D. Tactile sensor fabrication and hardware setup

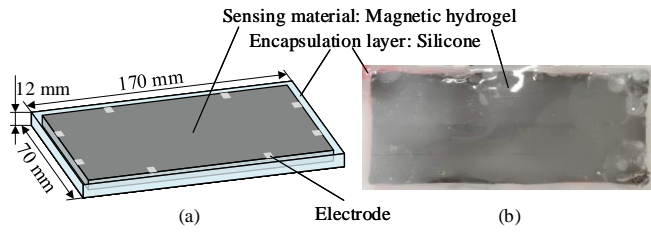


Fig. 3: Illustration of an 8-Electrode EIT Tactile Sensor. (a) Schematic of the magnetic hydrogel-based EIT tactile sensor. (b) Photograph of the sensor.

The magnetic hydrogel composite was chosen as the sensing layer in this study mainly because of its improved mechanical stability and strong pressure-sensing performance when integrated with EIT [28]. As shown in Fig. 3, the tactile sensor is composed of three primary components: a silicone layer, a magnetic hydrogel sensing layer, and eight silver electrodes uniformly distributed along the boundaries. The sensor has overall dimensions of $160 \text{ mm} \times 70 \text{ mm} \times 12 \text{ mm}$, while the magnetic hydrogel layer measures $150 \text{ mm} \times 60 \text{ mm} \times 5 \text{ mm}$. Each of the 8 silver electrodes interfaces with the conductive layer through a contact area of $5 \text{ mm} \times 5 \text{ mm}$. To prevent moisture loss, the sensing material is encapsulated using Ecoflex 30 silicone rubber, which helps maintain the hydration state of the hydrogel and ensures the long-term stability of its performance. Components A and B of the silicone were mixed at a 1:1 weight ratio, stirred thoroughly, and degassed to eliminate air bubbles. The mixture was then cast into a mold, fully encapsulating the magnetic hydrogel. After curing at room temperature for 2–3 hours, a protective silicone layer was formed, ensuring the hydrogel's stability and functionality.

The data acquisition circuit is based on the AD5940 impedance measurement IC, which supports signal generation and measurement bandwidth up to 200 kHz [29]. A

40 kHz excitation frequency balances speed and accuracy, consistent with prior EIT systems [30], [31]. Multiplexers (ADG706) enable sequential addressing of electrodes, and a 4-wire measurement approach captures impedance changes [29], acquiring unique pairwise measurements without repetition. A microcontroller (STM32) coordinates the multiplexers, the AD5940, and data transmission to a computer. Further implementation details are provided in [32].

III. TACTILE SENSOR EXPERIMENT

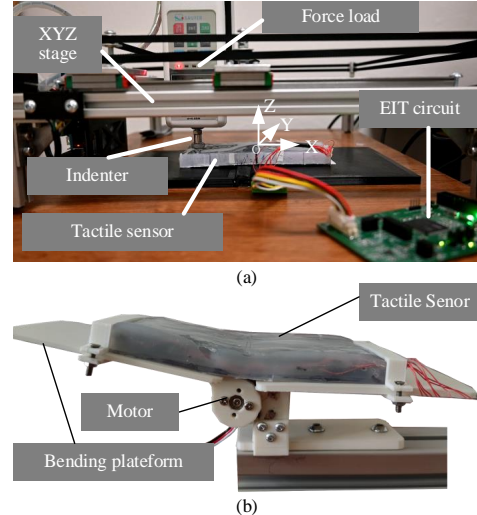


Fig. 4: Experimental setups for (a) Touch test; (b) Bending test.

Experiments were conducted to evaluate the touch sensing and bending angle estimation capabilities of the proposed EIT-based tactile sensor. As shown in Figure 4 (a), a controlled indentation test was performed using an experimental setup where the sensor was fixed horizontally, and an indenter was mounted on a computer-controlled XYZ stage. The stage was programmed to move along the z-axis to apply indentation forces, which were precisely measured using an inline commercial force gauge (Sauter FH100). To evaluate the sensor's response to mechanical deformation, a bending test platform was developed, as shown in Figure 4 (b). The setup consists of a 3D-printed support structure with a mounted servo motor (ST3025, Waveshare Electronics, China) that drives a hinged mechanism to induce controlled bending of the tactile sensor. The sensor is fixed at both ends, and the central region is deflected by rotating the motor to predefined angles. The bending platform ensures repeatable and adjustable deformation, enabling systematic collection of EIT data under various bending conditions. The bending angle is precisely controlled via the motor, allowing synchronization between mechanical input and impedance measurement for training and validation purposes.

A. Single-touch indentation test

The sensor's touch localization accuracy was evaluated by measuring the error between the reconstructed compressed area's centroid and the actual indenter position. A 15 mm

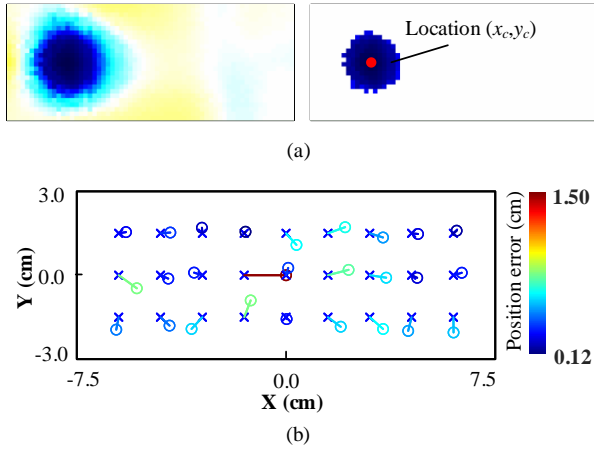


Fig. 5: Touch position error results.

diameter indenter applied a constant 10 N force at 27 different positions, spaced 15 mm apart along both the x- and y-axes. The touch location was determined using the method described in [32]. The touch positions are estimated by computing the centroid (x_c, y_c) of the reconstructed image, as shown in Figure 5 (a). Specifically, for the post-processed output, the centroid is calculated using a weighted average of pixel coordinates, where the weights correspond to the pixel intensities. This can be expressed as:

$$(x_c, y_c) = \left(\frac{\sum_i P_i x_i}{\sum_i P_i}, \frac{\sum_i P_i y_i}{\sum_i P_i} \right) \quad (3)$$

Here, P_i denotes the pixel value at coordinate (x_i, y_i) in the post-processed image. As shown in Figure 5(b), the error vectors represent the differences between the actual touch positions and the estimated locations. For each indentation point, we collected 8 repeated samples, resulting in an average localization error of 4.8 ± 2.8 mm.

B. State classification test

To classify different sensor interaction states (touch, bending, and idle), a supervised learning strategy was employed. The dataset consisted of 1,080 labeled samples, evenly distributed across the three classes to ensure balanced training. The bending class included 360 samples, each corresponding to a bending angle randomly selected within the range of -20° to 50° . The touch class comprised 360 samples captured from randomly chosen contact locations on the sensor surface, ranging from single-point to four-point touch. The idle class included 360 samples representing the no-action condition of the sensor. The dataset was randomly partitioned into 60% for training, 20% for validation, and 20% for testing. The deep neural network mentioned in the Figure 2 was trained using the sparse categorical cross-entropy loss function, with a batch size of 64, over 150 epochs to optimize classification performance.

The classification performance on the test set is summarized in the normalized confusion matrix shown in Figure 6. The model achieved high accuracy across all classes. This is attributed to the strong and distinctive features of

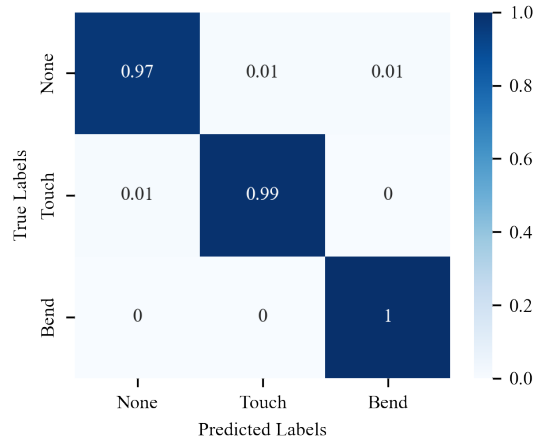


Fig. 6: Normalized confusion matrix for touch, bending, and idle state classification on test dataset.

bending-induced signals, which introduce significant static impedance changes that are easily distinguishable from other states. In contrast, minor misclassifications occurred between the touch and idle (none) classes. Specifically, 1% of the idle samples were misclassified as touch, and a similar proportion of touch samples were incorrectly labeled as idle. This confusion likely stems from the ill-posed nature of EIT reconstruction, where system noise and reconstruction artifacts—especially under low-contrast conditions—can produce localized patterns resembling touch inputs. This makes weak touch signals difficult to distinguish from background noise in the idle state. Despite this, the classifier still achieved over 97% accuracy for the idle class and 99% for the touch class, demonstrating robust performance across varying sensor interaction conditions.

C. Bending test

To establish a quantitative relationship between sensor voltage changes and bending angles, we adopted a data-driven approach that combines feature selection with linear regression modeling from the scikit-learn [26]. The model was trained using 360 bending samples, where the input features correspond to the EIT voltage change, and the output labels represent the ground-truth bending angles in degrees. The performance of this approach was evaluated through comprehensive testing of real-time angle prediction capabilities.

Figure 7 (a) presents the real-time prediction results obtained during a continuous bending sequence. The predicted angles demonstrate excellent tracking of the actual servo angles, maintaining accuracy even during dynamic transitions. This real-time performance is further validated by the correlation analysis, which displays the relationship between predicted and actual angles across the entire test dataset. The regression model achieved a high coefficient of determination ($R^2 = 0.997$) with a root mean square error (RMSE) of 0.90° , confirming both the accuracy and robustness of the proposed approach in capturing bending behavior. The real-time

response characteristics of our system during the bending test are demonstrated in the accompanying video, providing visual confirmation of the system's dynamic performance capabilities.

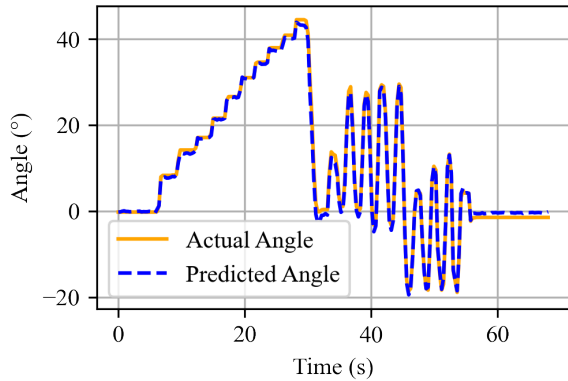


Fig. 7: Bending angle prediction validation.

D. Touch test

To evaluate the effectiveness of the proposed dynamic adaptive reference strategy, we conducted comprehensive touch mapping experiments under various bending conditions. The experimental setup employed the previously described bending apparatus to control precise angles, while touch stimuli were applied using a cylindrical indenter with a 15 mm diameter. Figure 8 presents the ground truth locations for one- to four-point touches on the sensor surface.

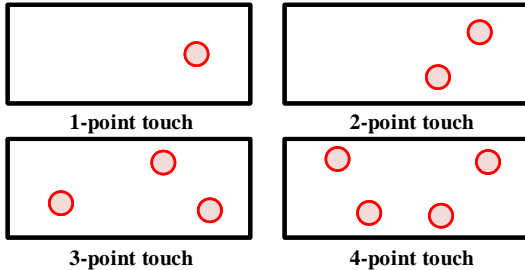


Fig. 8: Illustration of multi-point touch locations on the sensor surface.

The performance of our dynamic reference update method was systematically compared to conventional reconstruction approaches lacking reference adaptation. Figure 9 presents single-point touch reconstruction results at various bending angles for three methods: (i) static reference (left column), which does not update the reference during bending; (ii) dynamic reference (middle column), the proposed approach that updates the reference continuously as bending occurs; and (iii) dynamic reference with post-processing (right column), which applies an additional filtering step to the dynamic-reference reconstructions to enhance spatial clarity for potential multi-touch scenarios further. With the static reference method, touch localization is partially maintained

at small bending angles (e.g., -10° and 0°) but suffers from reduced clarity and precision. As bending exceeds 20° , reconstruction quality deteriorates markedly, with indistinct localization and strong background artifacts. The dynamic reference method mitigates these effects, preserving clearer and more accurate localization across all bending states. The addition of post-processing yields sharply defined, artifact-free contact regions. This qualitative im-

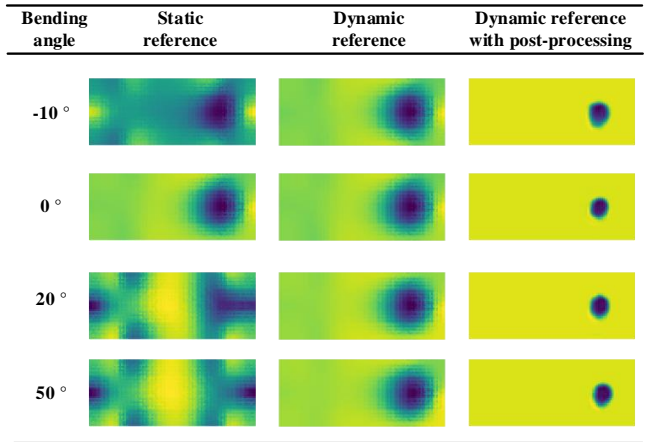


Fig. 9: Single point touch mapping under different bending angles with original and dynamic adaptive reference methods.

provement is supported by quantitative analysis using the structural similarity index (SSIM): the proposed approach with post-processing achieves an average SSIM of 0.94, compared to 0.29 for the static reference and 0.71 for the dynamic reference without post-processing. These results confirm that dynamic reference updating, especially when combined with post-processing, effectively compensates for bending-induced reference shifts and preserves spatial fidelity in flexible tactile sensing.

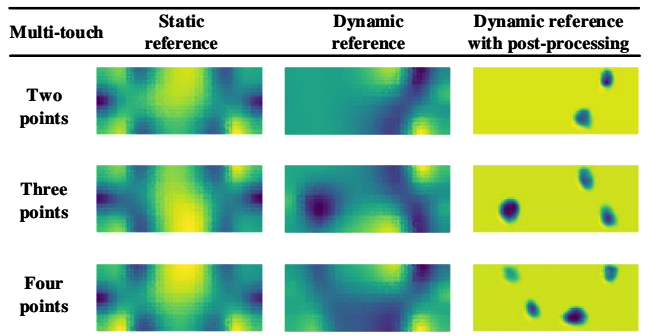


Fig. 10: Multi-point touch mapping at 30 degree bending with original and dynamic adaptive reference methods.

To assess the method's capability under more complex conditions, we tested two-, three-, and four-point contact scenarios (Figure 8) at bending angles up to 30° . The corresponding reconstruction results are shown in Figure 10. The static reference method fails to separate individual con-

tacts, producing merged and distorted regions. The dynamic reference approach improves separation but still exhibits residual artifacts. With post-processing, the proposed method achieves clear and distinct localization of all contact points, as reflected by the highest average SSIM (0.80) compared to the static reference (0.11) and dynamic reference without post-processing (0.47). This represents a notable advancement in flexible tactile sensing performance.

E. Real-time demonstration of touch and bending sensing

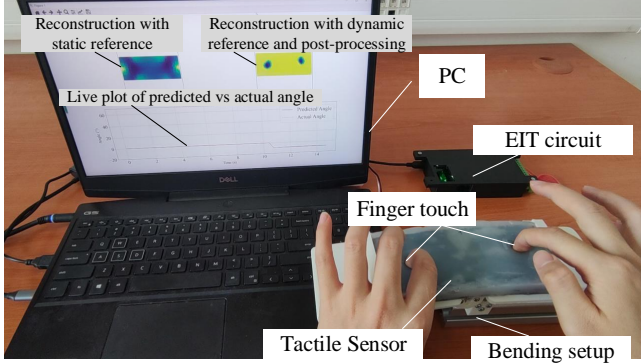


Fig. 11: Experimental setup for real-time bend angle prediction and touch detection.

To validate the proposed EIT-based sensing framework in a real-world setting, we conducted a real-time experiment involving both bending and multi-point touch interactions. This setup includes a flexible EIT-based tactile sensor mounted on a motorized bending platform. The EIT circuit acquires impedance measurements, which are transmitted to a PC for real-time processing. The display shows the reconstruction using the static reference alone and the dynamic reference combined with post-processing, and a plot of predicted versus actual bending angles over time. This configuration enables evaluation of both touch and deformation sensing performance.

As shown in Figure 12(a), we compare the touch reconstructions without the proposed framework (using a static reference) against the results produced by our proposed dynamic adaptive reference method. Four representative time points are selected, corresponding to various bending angles and multi-touch conditions: (a1) -10° with two-point touch, (a2) 20° with three-point touch, (a3) 40° with four-point touch, and (a4) 0° with four-point touch. At lower bending angles, such as in (a1) and (a4), the static reference method can roughly localize the touch positions, but significant artifacts and shape distortion are still visible. As the bending angle increases (e.g., (a2) and (a3)), these distortions become more severe, and the reconstruction fails to represent the true contact locations, especially under large deformations. In contrast, our proposed framework effectively compensates for bending-induced signal coupling, yielding accurate and artifact-free touch mappings across all configurations.

Figure 12(b) further validates the system's capability to estimate the bending angle and sense multiple touch points

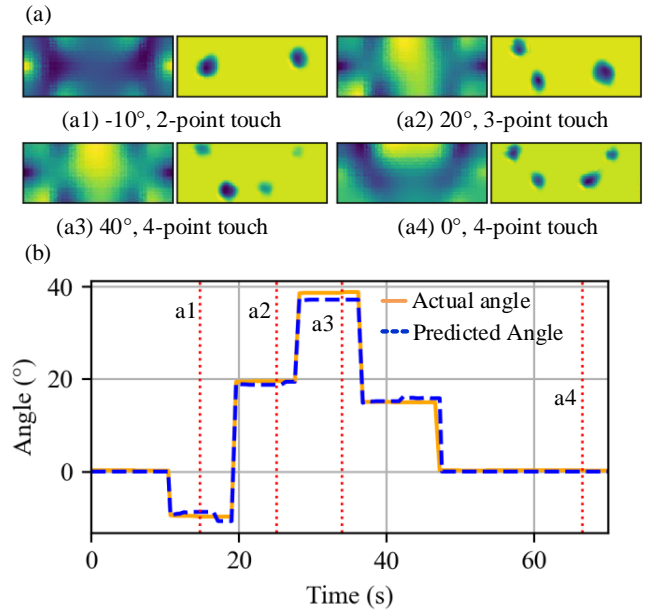


Fig. 12: Real-time touch and bending sensing results.

in real time. The predicted bending angles closely follow the actual servo motor trajectory, with the key time points (indicated by dashed lines) aligning well with the moments of touch shown in (a).

The framework demonstrates real-time processing capabilities for both touch mapping and angle prediction. It establishes the feasibility of the proposed EIT-based sensing approach for applications requiring both tactile and deformation feedback in flexible robotic systems.

IV. CONCLUSION

This work presents a robotic skin that leverages EIT for both touch sensing and bending angle estimation. By introducing a dynamic reference strategy with adaptive signal management, the system effectively handles deformation-induced reference shifts, enabling robust operation under dynamic conditions. A state classification network, enhanced by a linear voltage-to-image embedding, accurately distinguishes between touch, bending, and idle states. For quantitative analysis, a regression model estimates bending angles, while touch locations are mapped through EIT reconstruction followed by lightweight convolutional post-processing to refine spatial resolution.

The experimental results confirm the sensor's capability to track continuous bending and resolve multi-touch inputs under various deformation conditions. Notably, the system achieves high localization precision and bending prediction accuracy, demonstrating its feasibility for real-world deployment in robotic applications.

A limitation of the current method is that it relies on sequential reference updates, which restricts fully simultaneous decoupling of touch and bending signals. Despite this, the proposed dual-reference strategy and adaptive classification framework significantly improve robustness and accuracy in

dynamic tactile sensing. Future work will explore alternative approaches to enable simultaneous detection of complex deformations (such as torsional and shear deformations), further advancing the capabilities of robotic skin systems.

The demonstrated framework holds strong potential for whole-body tactile sensing in humanoid and soft robots, enabling more nuanced physical and social interactions and further advancing the capabilities of robotic skin systems.

REFERENCES

- [1] C. Bartolozzi, L. Natale, F. Nori, and G. Metta, “Robots with a sense of touch,” *Nature materials*, vol. 15, no. 9, pp. 921–925, 2016.
- [2] R. Dahiya, D. Akinwande, and J. S. Chang, “Flexible electronic skin: From humanoids to humans [scanning the issue],” *Proceedings of the IEEE*, vol. 107, no. 10, pp. 2011–2015, 2019.
- [3] G. Cannata, M. Maggiali, G. Metta, and G. Sandini, “An embedded artificial skin for humanoid robots,” in *2008 IEEE International conference on multisensor fusion and integration for intelligent systems*. IEEE, 2008, pp. 434–438.
- [4] P. Mittendorfer and G. Cheng, “Humanoid multimodal tactile-sensing modules,” *Robotics, IEEE Transactions on*, vol. 27, no. 3, pp. 401–410, 2011.
- [5] G. Cheng, E. Dean-Leon, F. Bergner, J. R. G. Olvera, Q. Leboulet, and P. Mittendorfer, “A comprehensive realization of robot skin: Sensors, sensing, control, and applications,” *Proceedings of the IEEE*, vol. 107, no. 10, pp. 2034–2051, 2019.
- [6] P. Maiolino, M. Maggiali, G. Cannata, G. Metta, and L. Natale, “A flexible and robust large scale capacitive tactile system for robots,” *Sensors Journal, IEEE*, vol. 13, no. 10, pp. 3910–3917, 2013.
- [7] D. Silvera-Tawil, D. Rye, and M. Velonaki, “Artificial skin and tactile sensing for socially interactive robots: A review,” *Robotics and Autonomous Systems*, vol. 63, pp. 230–243, 2015.
- [8] G. Pang, G. Yang, and Z. Pang, “Review of robot skin: A potential enabler for safe collaboration, immersive teleoperation, and affective interaction of future collaborative robots,” *IEEE Transactions on Medical Robotics and Bionics*, vol. 3, no. 3, pp. 681–700, 2021.
- [9] T. G. Thuruthel, B. Shih, C. Laschi, and M. T. Tolley, “Soft robot perception using embedded soft sensors and recurrent neural networks,” *Science Robotics*, vol. 4, no. 26, p. eaav1488, 2019.
- [10] K. Noda, E. Iwase, K. Matsumoto, and I. Shimoyama, “Stretchable liquid tactile sensor for robot-joints,” in *2010 IEEE International Conference on Robotics and Automation*. IEEE, 2010, pp. 4212–4217.
- [11] M. Totaro, A. Mondini, A. Bellacicca, P. Milani, and L. Beccai, “Integrated simultaneous detection of tactile and bending cues for soft robotics,” *Soft robotics*, vol. 4, no. 4, pp. 400–410, 2017.
- [12] M. S. Sarwar, Y. Dobashi, C. Preston, J. K. Wyss, S. Mirabbasi, and J. D. W. Madden, “Bend, stretch, and touch: Locating a finger on an actively deformed transparent sensor array,” *Science advances*, vol. 3, no. 3, p. e1602200, 2017.
- [13] Y. Zhang, M. Shafiei, J. Z. Wen, Z. Abbasi, and C. L. Ren, “Simultaneous detection of pressure and bending using a microwave sensor with tag and reader structure,” *IEEE Transactions on Instrumentation and Measurement*, vol. 72, pp. 1–11, 2023.
- [14] T. Kim, S. Lee, T. Hong, G. Shin, T. Kim, and Y.-L. Park, “Heterogeneous sensing in a multifunctional soft sensor for human-robot interfaces,” *Science robotics*, vol. 5, no. 49, p. eabc6878, 2020.
- [15] D. H. Lee, J. C. Yang, J. Y. Sim, H. Kang, H.-R. Kim, and S. Park, “Bending sensor based on controlled microcracking regions for application toward wearable electronics and robotics,” *ACS Applied Materials & Interfaces*, vol. 14, no. 27, pp. 31312–31320, 2022.
- [16] W. Xin, F. Zhu, P. Wang, Z. Xie, Z. Tang, and C. Laschi, “Electrical impedance tomographic shape sensing for soft robots,” *IEEE Robotics and Automation Letters*, vol. 8, no. 3, pp. 1555 – 1562, 2023.
- [17] T. C. Yu, R. Arakawa, J. McCann, and M. Goel, “uknit: A position-aware reconfigurable machine-knitted wearable for gestural interaction and passive sensing using electrical impedance tomography,” in *Proceedings of the 2023 CHI Conference on Human Factors in Computing Systems*, 2023, Conference Proceedings, pp. 1–17.
- [18] H. Dong, X. Wu, D. Hu, Z. Liu, F. Giorgio-Serchi, and Y. Yang, “Learning-enhanced electronic skin for tactile sensing on deformable surface based on electrical impedance tomography,” *IEEE Transactions on Instrumentation and Measurement*, vol. 74, pp. 1–9, 2025.
- [19] H. Park, W. Kim, S. Jeon, Y. Na, and J. Kim, “Graph-structured super-resolution for geometry-generalized tomographic tactile sensing: Application to humanoid faces,” *IEEE Transactions on Robotics*, vol. 41, pp. 558 – 572, 2024.
- [20] Y. Kato, T. Mukai, T. Hayakawa, and T. Shibata, “Tactile sensor without wire and sensing element in the tactile region based on eit method,” *SENSORS, 2007 IEEE*, pp. 792–795, 2007.
- [21] A. Nagakubo, H. Alirezaei, and Y. Kuniyoshi, “A deformable and deformation sensitive tactile distribution sensor,” in *2007 IEEE International Conference on Robotics and Biomimetics (ROBIO)*, 2007, Conference Proceedings, pp. 1301–1308, eIT.
- [22] J. Avery, M. Runciman, A. Darzi, and G. P. Mylonas, “Shape sensing of variable stiffness soft robots using electrical impedance tomography,” in *2019 International Conference on Robotics and Automation (ICRA)*. IEEE, 2019, pp. 9066–9072.
- [23] D. Silvera-Tawil, D. Rye, M. Soleimani, and M. Velonaki, “Electrical impedance tomography for artificial sensitive robotic skin: a review,” *IEEE Sensors Journal*, vol. 15, no. 4, pp. 2001–2016, 2015.
- [24] A. Adler, T. Dai, and W. R. Lionheart, “Temporal image reconstruction in electrical impedance tomography,” *Physiological measurement*, vol. 28, no. 7, p. S1, 2007.
- [25] M. Cheney, D. Isaacson, J. C. Newell, S. Simske, and J. Goble, “Noser: An algorithm for solving the inverse conductivity problem,” *International Journal of Imaging systems and technology*, vol. 2, no. 2, pp. 66–75, 1990, linear.
- [26] F. Pedregosa, G. Varoquaux, A. Gramfort, V. Michel, B. Thirion, O. Grisel, M. Blondel, P. Prettenhofer, R. Weiss, V. Dubourg, *et al.*, “Scikit-learn: Machine learning in python,” *The Journal of machine Learning research*, vol. 12, pp. 2825–2830, 2011.
- [27] H. Chen, X. Yang, J. Geng, G. Ma, and X. Wang, “A convolutional neural network based electrical impedance tomography method for skin-like hydrogel sensing,” pp. 178–183, 5–9 Dec. 2022 2022.
- [28] B. Li, X. Yang, H. Chen, C. Xu, and X. Wang, “Flexible tactile sensing of magnetic hydrogel composites based on electrical impedance tomography,” *Journal of Intelligent Material Systems and Structures*, p. 1045389X241280631, 2024.
- [29] Analog Devices, *High Precision, Impedance, and Electrochemical Front End AD5940/5941 (Data Sheet)*, Analog Devices, Norwood, MA, USA, 2020. [Online]. Available: <https://www.analog.com/media/en/technical-documentation/data-sheets/AD5940-5941.pdf>
- [30] G. Ma, Z. Hao, X. Wu, and X. Wang, “An optimal electrical impedance tomography drive pattern for human-computer interaction applications,” *IEEE Transactions on Biomedical Circuits and Systems*, vol. 14, no. 3, pp. 402–411, 2020.
- [31] Y. Zhang, R. Xiao, and C. Harrison, “Advancing hand gesture recognition with high resolution electrical impedance tomography,” in *Proceedings of the 29th Annual Symposium on User Interface Software and Technology*. ACM, 2016, pp. 843–850.
- [32] H. Chen, X. Yang, P. Wang, J. Geng, G. Ma, and X. Wang, “A large-area flexible tactile sensor for multi-touch and force detection using electrical impedance tomography,” *IEEE Sensors Journal*, vol. 22, no. 7, pp. 7119–7129, 2022.